水平管群を流下する液膜表面波の生成とガス吸収促進の機構解明

seems to decrease with increasing *Re*.

At *Re* above 40, waves are highly unstable in the face of 3-D perturbations of smaller spanwise intervals of $\lambda_{z,ndl} \approx 2$ cm, and continuously evolve transverse wavefront modulations. The wavefronts show sinusoidal shapes with small amplitudes at the first stage. Curves bulging downward on the sinusoids then continuously expand into horseshoe-shapes while those bulging upward flatten out and then reduce the widths of the flat parts (Figure 7d). Finally, the horseshoes extend their legs and split the legs off the flat parts, which disintegrate into clusters of dimples. The horseshoes keep holding the teardrop-hump/capillary-ripple structures (Figures 7d, 7e and 9). When spanwise perturbations of $\lambda_{z,ndl} = 1$ cm are imposed on the film flow at *Re* ≈ 90, the downward curves at 2-cm intervals on the wavefronts grow more rapidly, developing into horseshoes at 2-cm intervals associated with the disintegration of slowly growing curves between the horseshoes into the dimples (Figure 7e). At larger *Re*, the downward curves at 1-cm intervals grow so rapidly that horseshoes occur at random intervals of 1 cm, 2 cm, or values in between. These observations show that the fastest growing transverse wavelength is somewhere near 2 cm at *Re* above 40, and it slightly decreases with increasing *Re*.

At *Re* near and below 40, the sinusoidal wavefront modulations are followed by the evolution of curves bulging downward, with upward curves flattening out between the downward curves (Figure 7c). The evolution of the downward curves then becomes saturated and the waves travel downstream in a quasi-stationary state, showing that deformations of the wavefronts are limited to low levels.

This surface waves behavior changes with the frequency of the imposed perturbations. High-frequency perturbations excite closely packed waves and cause them to transform into highly 3-D solitary waves with large separations after complex interactions and coalescence. At very low frequencies, the waves are excited by large separations, and a new wave rapidly develops between the former waves. Then complex interactions and coalescence occur between the former and the latter, causing highly 3-D wavefront patterns. The wave behaviors described in this article are observed at the frequencies where waves are excited to have mostly separations of λ_{hmp} = 2–5 cm. Naturally occurring 3-D waves seem to have comparable wavelengths after wave coalescence events (Figure 6).

Chang and Demekhin (2002) carried out a preliminary stability analysis and numerical experiments in a wide range of *Re* by solving the 3-D generalized Kuramoto-Sivashinsky equation, and presented four wave dynamics regimes. The second and third wave regimes seem

to predict the previously mentioned experimental observations of 3-D wave behaviors. At the *Re* range of the second regime, 2-D humps develop transverse modulations to some limiting levels without disintegration, whereas the disintegrations of humps into disconnected 3-D humps, or *scallop waves*, occur at larger *Re* in the third regime.

Transverse propagation of wavefront modulation

A single positive perturbation causes a single curve to bulge downward on every 2-D wavefront. This curve then increases in its spanwise width, but not in its height, to induce a gentle modulation with large transverse wavelengths of $\lambda_z \approx 4$ cm at *Re* near 20 or smaller (Figure 8a). The modulations propagate transversely on wavefronts in different behaviors at *Re* above 20 (Figure 8b). Two curves appear on the both sides of the first one excited by the perturbation, and then two more appear on the sides of the second ones. All curves eventually evolve into horseshoes at intervals of about 1.5–2.0 cm at *Re* above 40, but the evolution of the curves saturates at *Re* near 40 or smaller.

A single negative perturbation excites a single bend of the wavefront, followed by the flat top of the bend expanding horizontally at *Re* near 20 or smaller (Figure 8c). The expansion of the flat top is soon saturated at *Re* near 40. At *Re* above 40, the bend with the short flat top accompanies the growth of the downward curves on both sides, coupled with the eventual splitting of the flat top off the two curves. This expansion of the flat part indicates that the waves are not unstable in the face of this single-point perturbation at *Re* near 20 or smaller.

Structure of horseshoe and partial wave disintegration

Horseshoes have gently curving heads that extend oblique legs to short distances upward at *Re* near 40. However, they demonstrate increase in the head curvatures and elongation of oblique legs to greater distances at a larger *Re*, as shown in Figure 9. The horseshoes have teardrop-hump/capillary-ripple structures throughout their wavefronts even after they increase the curvatures of the heads and extend the long oblique legs. The horseshoe speed, c, is calculated to be a multiple of the constant frequency, f, and the separation λ_{hmp} between the humps, and variations of the separation λ_{hmp}, which represent variations of the speed c, are shown in Figure 10. The horseshoe heads and the flat parts between them first accelerate to the maxima as the horseshoes are growing, and then gradually decelerate as the horseshoes split off the flat parts that disintegrate into dimples. The heads accelerate faster than the flat parts, which

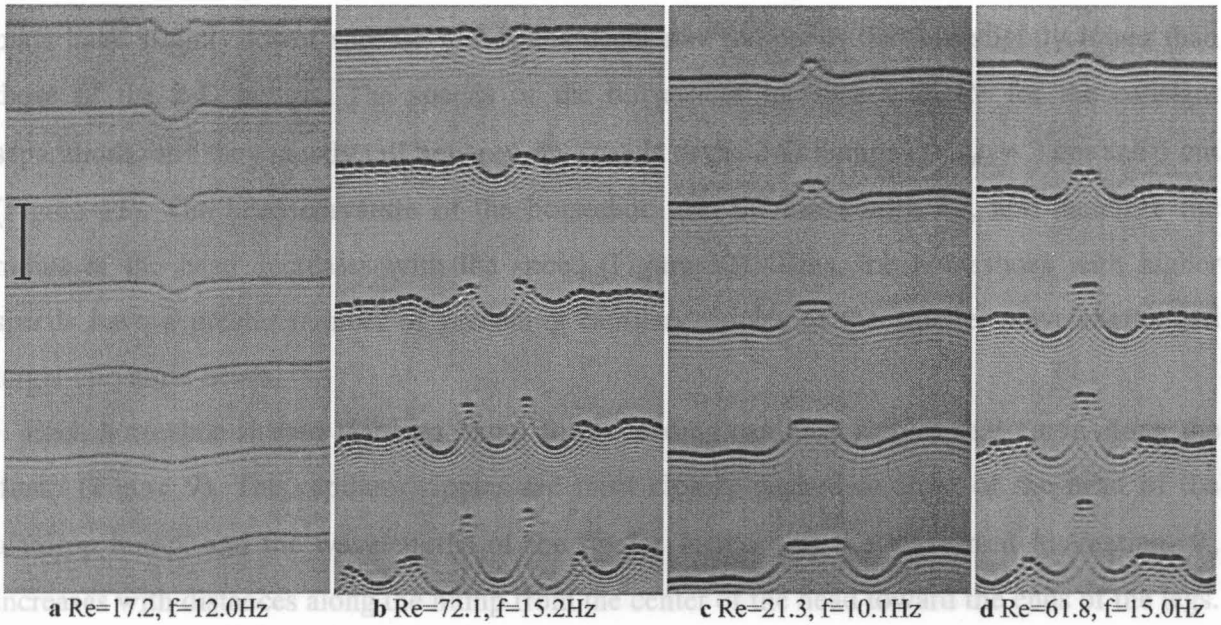

a Re=17.2, f=12.0Hz **b** Re=72.1, f=15.2Hz **c** Re=21.3, f=10.1Hz **d** Re=61.8, f=15.0Hz

Fig. 8. Shadow images of waves excited with single positive (**a**, **b**) or negative (**c**, **d**) spatial perturbations and time-periodic perturbations.

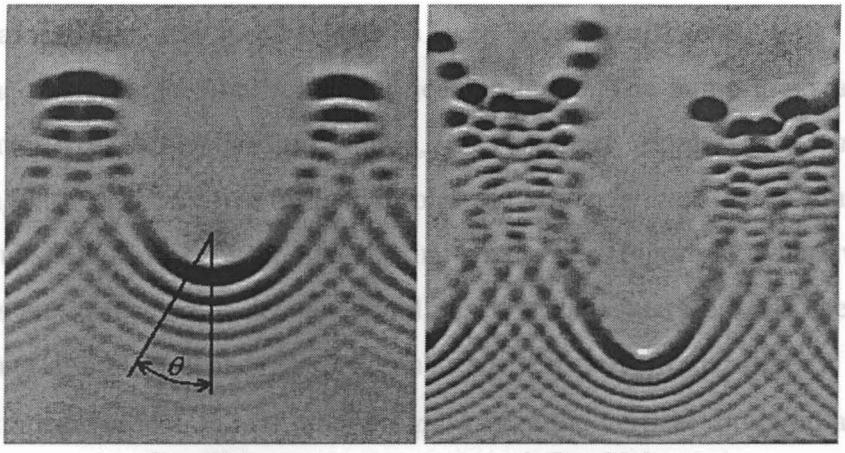

a Re=50.1 **b** Re=88.6

Fig. 9. Blow-up images of horseshoe-shaped waves and wave disintegrations into dimples between the horseshoes at $\lambda_{z,ndl}$ = 2 cm. Dark horseshoe-shaped strips represent valleys of capillary ripples, and clusters of dark spots represent the dimples.

increase the difference in speed between the heads and the flat parts, and the maximum speeds of the heads are slightly higher than those of the fully developed 2-D humps, whereas the flat parts have slightly lower speeds. The heads decelerate to speeds that are slightly lower than those of the 2-D humps. The speeds of the horseshoes increase with *Re* for the constant separations, and they mostly fall between the speeds of the 2-D humps at λ_{hmp} = 3 cm and 5 cm (Figure 11). The head curvature of the horseshoe also increases with *Re*, and therefore the radius of the head decreases with the speed (Figure 12). Thus, the horseshoes with higher speeds have a greater number of preceding capillary ripples of the smaller wavelengths and larger curvature heads.

Each horseshoe-shaped teardrop hump forms leading capillary ripples that curve along the hump (Figure 9). The capillary ripples are most closely packed in front of the head of the teardrop hump, and the wavelengths of the ripples increase as the wavefront inclination, θ, increases with distances along the hump from the center of the head toward the ends of the legs. The wavelength of capillary ripples is inversely proportional to $cos\theta$, as shown in Figure 13, where θ is the angle between the normal to the curving wavefront and the vertical (see Figure 9). The linear increase in the capillary ripple's wavelength with $1/cos\theta$ is explained as the following by invoking the theoretical correlation of capillary waves on shallow water (Dias and Kharif, 1999), which shows that the wavelength is inversely proportional to the propagation velocity when the water depth is smaller than the wavelength. A horseshoe-shaped hump travels in the vertical direction at a speed c, and its steep front is sufficiently large to form capillary ripples on the thin residual film behind the leading hump. The hump looks as if it *pushes* the ripples (Brauer, 1956). Unlike the hump, the capillary ripples are *wave* and are not mass-carrying, and therefore two oblique ripples cause *interference* that produces checkerboard patterns on substrate films between neighboring horseshoes (Figure 9), where valleys and crests of the ripples are, respectively, deepened and raised at their intersections. The capillary ripples *propagate* in a directions that is perpendicular to their wavefronts, that is, the directions of angles, θ, with the vertical, though they are *pushed* in the vertical direction at the speed, c, of the horseshoe. As a result, the propagation velocity of the capillary ripples is calculated to be a multiple of c and $cos\theta$. The depth of the substrate film is smaller than the wavelength of the ripples, as shown in Figure 2, and finally the theoretical correlation (Dias and Kharif, 1999) can be applied to the capillary ripples of the horseshoe to derive the linear increase in the ripple's wavelength with $1/cos\theta$.

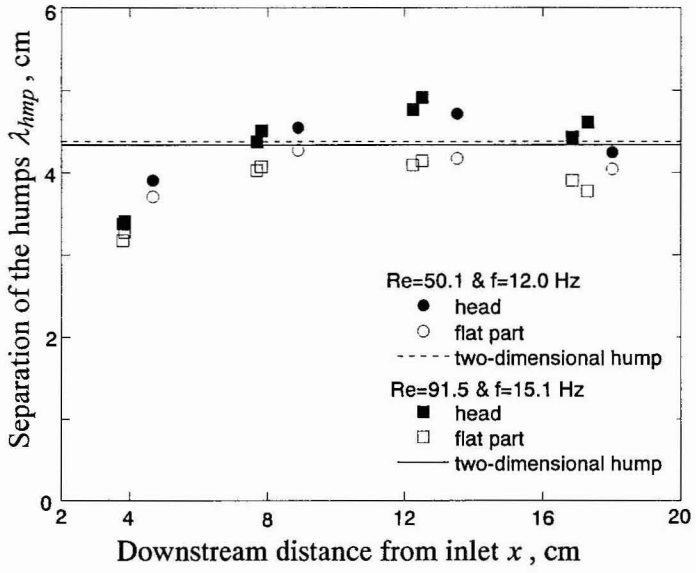

Fig. 10. Downstream distance and variations of separation λ_{hmp} of horseshoe heads and of flat parts between the horseshoes at constant frequencies.

The separations between fully developed two-dimensional waves are calculated from the empirical correlation by Nosoko et al. (1996).

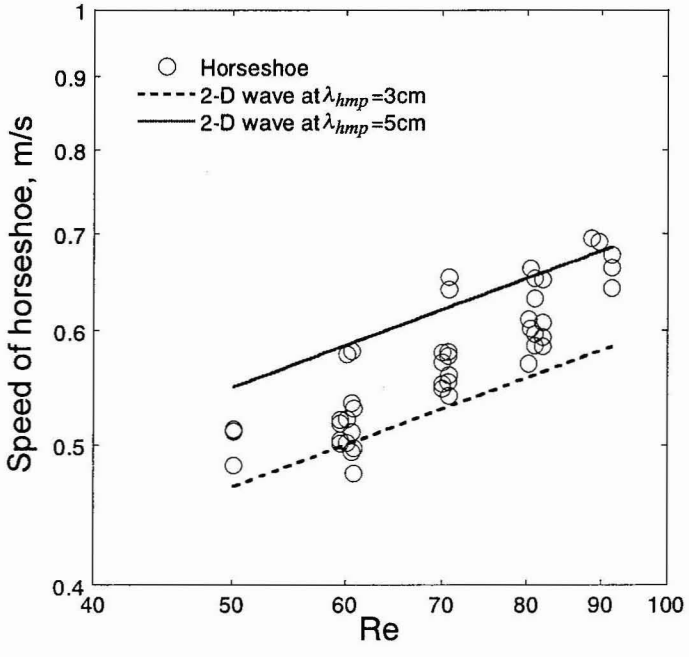

Fig. 11. Variation of horseshoe-shaped wave speed with *Re*.

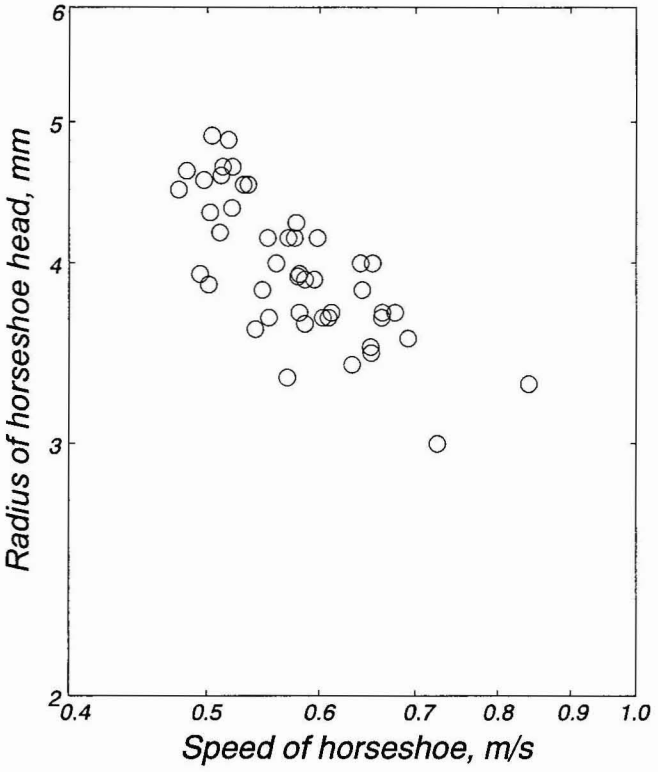

Fig. 12. Variation of radius of horseshoe head wavefront with its speed. The radii are measured on the darkest strips of shadows which represent the deepest valleys in front of horseshoes.

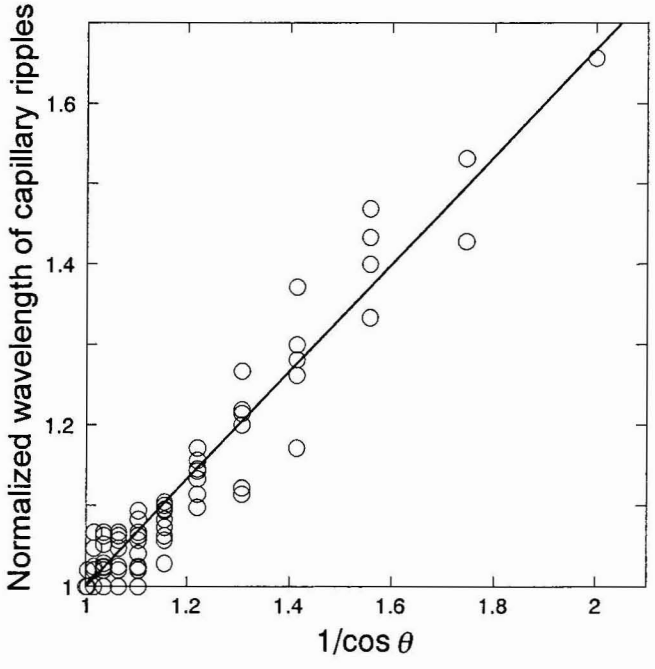

Fig. 13. Linear relationship between wavelength λ_{rpl} of capillary ripples and $1/cos\theta$. The wavelengths are normalized with respect to wavelengths at $\theta = 0$. The data are presented for Re=50–89 at f=12–15 Hz. The line is drawn to fit the data, passing through (1,1).

Interference also occurs between the flat capillary ripple and two oblique capillary ripples, respectively, that precede the flat part and the horseshoe legs (Figure 9). When the flat parts are not too short, dimples appear on the deepest valleys of the flat parts due to the *capillary instability* (described in the next subsection), which is associated with the wave interference (Figure 9b). The resulting clusters of dimples decelerate and split off the horseshoe legs (Figure 8d). Then the teardrop hump of the short flat wavefront and the preceding dimples gradually diminish, some of them fading away before the upstream hump catches up with them. At *Re* near 70 or larger, the capillary instability is so intense that the flat deepest valleys disintegrate into rows of dimples, releasing a few dimples from both ends of each row (Figure 9b). When the flat parts are short, such dimples do not appear on the deepest flat valleys (Figure 9a). Instead, the widths of the flat parts decrease.

The horseshoe shadows show that sharply slanting legs still hold teardrop-hump/capillary-ripple structures, but the legs form lighter strips on the screen, since the amplitudes of the capillary ripples and the heights of the hump peaks are much smaller than those of their head parts. The peak height of a teardrop hump monotonously decreases with the distance along its wavefront from the center of the head to the ends of the two legs. Teardrop humps of larger peaks form deeper valleys in front of the peaks as well as larger numbers of leading capillary ripples (Figure 9).

Capillary instability on deep valley

Dimples also appear on the deepest horizontal valleys in front of the teardrop humps at *Re* above 50, as shown in Figure 14. When only the temporal perturbations are imposed but the spanwise perturbations are not, transverse wavefront modulations start to grow later. At the final stage of 2-D wave development, dimples appear at nearly constant intervals on the deepest valleys, and then quickly spread throughout the valleys before transverse wavefront modulations become significant. Afterwards, the wavefronts increase the transverse modulation that develops into horseshoes at irregular transverse intervals and irregular growth rates, since spatial perturbations can originate from minute defects in the channel discharging the film and trigger the horseshoes. The dimples disappear on the curving heads of horseshoes, whereas they survive or are intensified on the horseshoe legs and on the flat parts between the horseshoes. The flat parts eventually split off from the horseshoes and disintegrate into dimples.

The valleys in front of teardrop humps deepen to form large surface curvatures at their

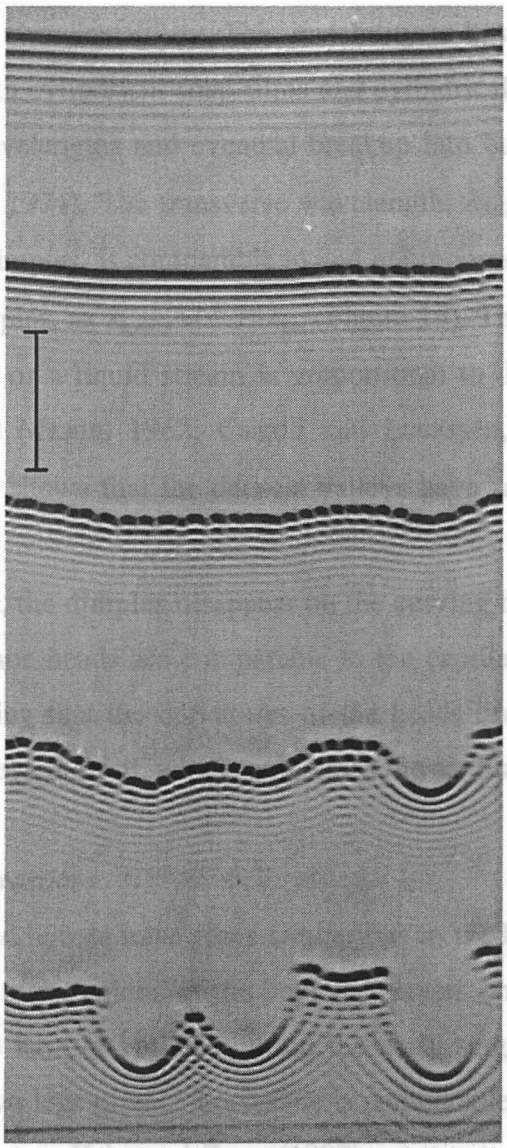

Fig. 14. Shadow images of waves excited with time-periodic perturbations and of dimples appearing on two-dimensional deep valleys. The snapshot captures the films at x=4.6–21.1 cm, and the bar is 2 cm long.

bottoms, which causes liquid-side negative pressure to build up due to capillary force, resulting in the occurrence of a new instability. This instability is basically the same as the capillary instability observed with cylindrical soap films and cylindrical liquid streams that demonstrate necking at constant wavelengths and eventual breakup into bubbles and droplets, respectively (Carroll and Lucassen, 1974). The transverse wavelength, $\lambda_{z,dmp}$, of this instability, that is, the intervals between the dimples, is comparable to and in proportion to the streamwise wavelength, λ_{rpl}, of the capillary ripples, as $\lambda_{z,dmp} = 1.15\lambda_{rpl}$ (Figure 15). The fastest growing wavelength of a cylindrical soap film or a liquid stream is proportional to the radius of the cylinder (Boys, 1959; Rumscheidt and Mason, 1962; Carroll and Lucassen, 1974). The linear relationship between $\lambda_{z,dmp}$ and λ_{rpl} shows that the deepest valleys have radii on their bottoms that are in proportion to λ_{rpl}.

As mentioned earlier, the dimples disappear on the curving horseshoe heads (Figure 14), and the radii of the horseshoe heads are comparable to the capillary constant of water (=3.8 mm) (see Figure 12), implying that the curvatures of the heads cause additional capillary pressure around the deepest valleys in front, which suppresses the capillary instabilities.

Similarities to hairpin vortices

The horseshoe-shaped humps have some similarities to the hairpin vortices developed in the laminar–turbulent transition regions of the boundary layers on walls. First, the horseshoes are similar in shape to the hairpin vortices during the early stages of development. Second, the distance between the two legs of each horseshoe is comparable to the distance between the two legs of each hairpin vortex. Krist and Zang (1987) constructed the birth of hairpin vortices in plane Poiseuille flow by analyzing computer simulation data. The top views of their hairpin vortices are similar in shape to those of the horseshoe-shaped humps presented here, though the hairpin vortices lift their head up off the wall so their legs make an angle with the wall. A few reports are available on experimental observations of the distance between the two legs of a hairpin vortex. Acarlar and Smith (1987) presented visualizations of counterrotating legs of hairpin vortices in a boundary layer on the wall at a momentum thickness Reynolds number of Re_θ =135, and Nishioka et al. (1981) reported measurements of velocity fluctuations caused by hairpin vortices in plane Poiseuille flow at Re_θ =667. Their visualizations and measurements show that the distances between the legs are approximately 1 cm. We measured spanwise distances between horseshoe legs at their ends and found that the distances are in the 0.9 – 1.6

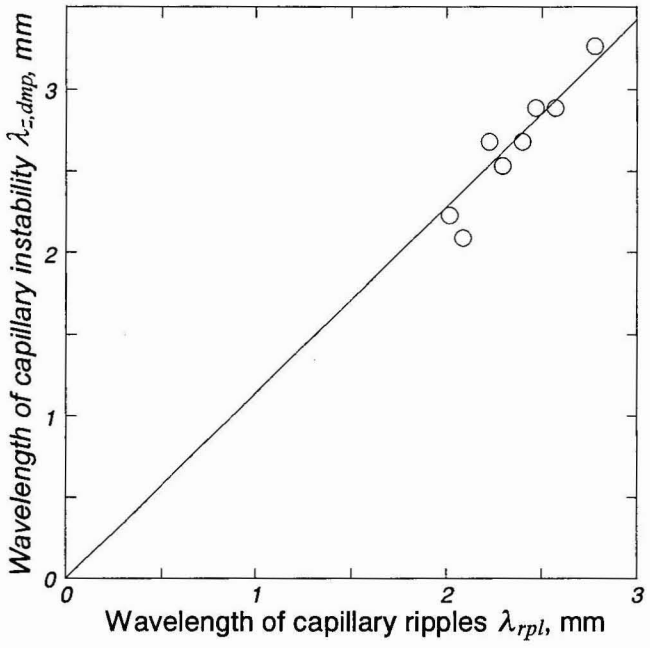

Fig. 15. Linear relationship between wavelength of capillary instability $\lambda_{z,dmp}$ and wavelength of capillary ripples λ_{rpl}.
The λ_{rpl} is determined by measuring the streamwise distances between the deepest valley and the next one. The correlation $\lambda_{z,dmp} = 1.15\lambda_{rpl}$ fits the experimental data.

cm range. These similarities may just be common characteristics of vortices subjected to near-wall shear flow, though such similarities disappear during the later stages when the hairpin vortices continue to grow, extending long streamwise legs, whereas the development of the horseshoe-shaped humps is limited to much smaller levels due to capillary force. The Re = 40, equal to Re_θ = 8, for the horseshoe humps is much smaller than the Re_θ for the hairpin vortices, suggesting that the effects of gravity that destabilize the 2-D humps are significant.

Wave dynamics and the associated mass transfer

It is interesting to note that there are large differences in the dynamics of surface waves between Re below 40 and above 40, and at the critical value of $Re \approx 40$, the slope of the Sh Re curve sharply changes. The waves at Re above 40 are distinguished from the waves at Re below 40 by the development of horseshoe waves and by wave disintegrations between the horseshoes into dimples. The horseshoes have the teardrop-hump/capillary-ripple structure (Figure 2), though the peaks of teardrop humps become smaller on the oblique legs of the horseshoes. Nagasaki et al. (2002) and Miyara (2000) demonstrated that weak vortices occur in teardrop humps. Yoshimura et al. (1996) showed that the vortices renew the film surface to greatly increase the mass transfer from the surface into the film, and these renewal effects monotonously increase with increasing height of the teardrop hump peak. Their findings may not be limited to 2-D waves as long as surface waves hold teardrop-hump/capillary-ripple structures. The wave disintegrations between horseshoes destroy the teardrop-hump/capillary-ripple structures, as well as the vortices inside the teardrop humps. At larger Re, the horseshoes have more sharply curved heads and longer oblique legs where the heights of the teardrop hump peaks are smaller than those of the heads, indicating that these low-peak teardrop humps hold vortices of low intensities. The partial destruction of the vortices and the diminishing vortices along the oblique wavefronts seem to be the main reasons why the slope of Sh Re curve is much smaller at $40 \lesssim Re \lesssim 400$ than at $Re \lesssim 40$.

Summary and Concluding Remarks

Although it is known that surface waves on falling films eventually become 3-D solitary waves downstream, their behaviors have not been fully understood. This article attempts to describe some features of the surface-wave dynamics on liquid films falling down a vertical plane. The experimental technique of controlling spatiotemporal perturbations allowed surface

waves to develop into 3-D waves at regular behaviors (Figure 7). A transition of the wave dynamics occurs at $Re \approx 40$. At Re below 40, 2-D waves are stable in the face of transverse perturbations of short wavelengths, but are unstable to long spanwise perturbations of about 2 cm or larger wavelengths, and develop transverse modulations of their wavefronts up to low levels (Figures 7a to 7c). At Re above 40, 2-D waves convert their wavefront modulations into a number of horseshoe-shapes, which afterward cause the waves between the horseshoes to disintegrate into clusters of dimples (Figures 7d and 7e). The horseshoes continue to hold the teardrop-hump/ capillary-ripple structures, with teardrop hump peaks decreasing along the oblique horseshoe legs (Figure 9). The horseshoe-shaped teardrop humps have larger curvature heads (Figure 12) and longer oblique legs at larger Re. The leading capillary ripples curving along a horseshoe increase their wavelengths with an increase in the ripple's wavefront inclination (Figure 13) as predicted by the linear theory of capillary waves on shallow water. Interference between a flat capillary ripple and two oblique capillary ripples occurs on substrate films between horseshoes, and capillary instabilities cause dimples on horizontal deep valleys in front of teardrop humps in the same way that a cylindrical soap film breaks up into a row of bubbles (Figures 14 and 15). The wave interferences and capillary instabilities cause clusters of dimples between the horseshoes, which eventually disintegrate and fade away. The horseshoe-shaped waves are similar in shape and size to hairpin vortices at their birth observed in the laminar–turbulent transition regions of boundary layers and of Poiseuille flow.

In the absence of controlled perturbations, waves appear on a smooth surface, soon causing complex interactions and coalescence between adjacent waves that develop into highly 3-D waves downstream (Figures 1 and 6). The 3-D waves at Re above 40 are distinguished from the waves at Re below 40 by a large number of horseshoes and dimples, suggesting that the features of the dynamics are basically the same as those of 3-D waves excited by the controlled perturbations.

Measurements of gas absorption into a falling film show that surface waves greatly enhance mass transfer, and that Sh increases with Re with a slope of 1.0 on a log-log scale at Re below 40, whereas the slope sharply decreases at $Re \approx 40$ to be 0.5 in $40 \lesssim Re \lesssim 400$ (Figure 4). Numerical simulations of film flow by Nagasaki et al. (2002) and Miyara (2000), and the experimental observations of the wave dynamics and the mass transfer by Nosoko et al. (1996) and Yoshimura et al. (1996) suggest that teardrop humps contain swirls or weak vortices inside (Figure 2) that greatly enhance the mass transfer from the surfaces into the films. The wave

dynamics mentioned earlier suggest that the initial rapid increase in *Sh* is spoiled at *Re* above 40 by the destruction of the vortices between horseshoes and the diminishing vortices in the oblique horseshoe legs.

Further investigations are required to fully understand the 3-D flow structures in the horseshoes, including the vortices. Numerical simulation techniques (Nagasaki et al., 2002) and velocity profile measurement methods (Karimi and Kawaji, 1998) developed recently seem to be useful in aiding such an understanding of flow structures.

Literature Cited

Acardar, M. S., and C. R. Smith, "A study of hairpin vortices in a laminar boundary layer. Part 2. Hairpin vortices generated by fluid injection," *J. Fluid Mech.* **175**, 43 (1987).

Alekseenko, S.V., Nakoryakov, V.E. and Pokusaev, B.G. *Wave flow of liquid films*, Begell House, New York (1994).

Alekseenko, S.V., Nakoryakov, V.E. and Pokusaev, B.G. "Wave formation on a vertical falling liquid film," *AIChE J.* **31**, 1446 (1985).

Bakopoulos, A. "Liquid-side controlled mass transfer in wetted-wall tubes," *Ger. Chem. Eng.*, **3**, 241 (1980).

Benjamin, T.B. "Wave formation in laminar flow down an inclined plane," *J. Fluid Mech.*, **2**, 554 (1957).

Bird, R.B., Stewart, W.E. and Lightfoot, E.N. *Transport Phenomena*, Wiley, New York (1960).

Boys, C.V. *Soap bubbles and the forces which mould them, Doubleday Anchor Books,* New York (1959).

Brauer, H. "Stromung und Warmeubergang bei Rieselfilmen," VDI, Forschungshelt, Vol. 457 (1956).

Carroll, B.J. and Lucassen, J. "Effect of surface dynamics on the process of droplet formation from supported and free liquid cylinders," *J. Chem. Soc., Faraday Trans. I*, **70,** 1228 (1974).

Chang, H.-C. "Wave evolution on a falling film," *Annu. Rev. Fluid Mech.* **26**, 103 (1994).

Chang, H.-C. and Demekhin, E.A. *Complex Wave Dynamics on Thin Films*, Elsevier, Amsterdam, The Netherlands (2002).

Chang, H.-C., Cheng, M., Demekhin, E.A. and Kopelevich, D.I. "Secondary and tertiary excitation of three-dimensional patterns on a falling film," *J. Fluid Mech.* **270**, 251 (1994).

Chang, H.-C., Demekhin, E.A. and Kalaidin, E. "Simulation of noise-driven wave dynamics on a falling film," *AIChE J.* **42**, 1553 (1996a).

Chang, H.-C., Demekhin, E.A., Kalaidin, E. and Ye, Y. "Coarsening dynamics of falling-film solitary waves," *Phys. Rev.* E, **54**, 1467 (1996b).

Chang, H.-C., Demekhin, E.A. and Kopelevich, D.I. "Nonlinear evolution of waves on a vertically falling film," *J. Fluid Mech.* **250**, 433 (1993a).

Chang, H.-C., Demekhin, E.A. and Kopelevich, D.I. "Construction of stationary waves on a falling film," *Comput. Mech.* **11**, 313 (1993b).

Chang, H.-C., Demekhin, E.A. and Saprikin, S.S. "Noise-driven wave transitions on a vertically falling film," *J. Fluid Mech.* **462**, 255 (2002).

Cheng, M. and Chang, H.-C. "Competition between subharmonic and sideband secondary instabilities on a falling film," *Phys. Fluids* **7**, 34 (1995).

Dias, F. and Kharif, C. "Nonlinear gravity and capillary-gravity waves," *Annu. Rev. Fluid Mech.* **31**, 301 (1999).

Emmert, R.E. and Pigford, R.L. "A study of gas absorption in falling liquid films," *Chem. Eng. Prog.,* **50**, 87 (1954).

Feind, K. "Strömungsuntersuchungen bei Gegenstrom von Rieselfilmen und gas in lotrechten Rohren," VDI- Forschungsheft, Vol. 481 (1960).

Fulford, G.D. "The flow of liquids in thin films," *Adv. Chem. Eng.*, **5**, 151 (1964).

Hikita, H., Nakanishi, K. and Kataoka, T. "Liquid phase mass transfer in wetted-wall columns," (in Japanese), *Chem. Eng.*, **23**, 459 (1959).

Himmelblau, D.M. "Diffusion of dissolved gases in liquid," *Chem. Rev.* **64**, 527 (1964).

Ho, L.W. and Patera, A.T. "A Legendre spectral element method for simulation of unsteady incompressible viscous free-surface flows," *Comput. Methods Appl. Mech. Eng* **80**, 355 (1990).

Jackson, L.J. "Liquid films in viscous flow," *AIChE J.* **1**, 231 (1955).

Joo, S.W. and Davis, S.H. "Instabilities of three-dimensional viscous falling films," *J. Fluid Mech.* **242**, 529 (1992a).

Joo, S.W. and Davis, S.H. "Irregular waves on viscous falling films," *Chem. Eng Commun.* **118**, 111 (1992b).

Joo, S.W., Davis, S.H. and Bankoff, S.G. "Long-wave instabilities of heated falling films: two-dimensional theory of uniform layers," *J. Fluid Mech.* **230**, 117 (1991).

JSME Data Book, *The Thermophysical Properties of Fluids*, Japan Society for Mechanical Engineers, Tokyo, Japan, p. 208 (1986).

Kamei, S. and Oishi, J. "Mass and Heat Transfer in a falling liquid film of wetted wall tower," *Memoirs Fac. Eng., Kyoto Univ.*, **17**, 277 (1956).

Kapitza, P.L. and Kapitza, S.P. "Wave flow of thin layers of a viscous fluid: Ⅲ. Experimental study of undulatory flow conditions," *Collected Papers of P.L. Kapitza,* Vol. 2, D. Ter Haar, ed., Pergamon, New York, p. 690 (1965).

Karimi, G. and Kawaji, M. "An experimental study of freely falling films in a vertical tube," *Chem. Eng. Sci.* **53**, 3501 (1998).

Krist, S.E. and Zang, T.A. "Numerical simulation of channel flow transition," NASA Tech. Pap. 2667 (1987).

Lamourelle, A.P. and Sandall, O.C. "Gas absorption into a turbulent liquid," *Chem. Eng. Sci.* **27**, 1035 (1972).

Lasheras, J.C. and Choi, H. "Three-dimensional instability of a plane free shear layer: an experimental study of the formation and evolution of streamwise vortices," *J. Fluid Mech.* **189**, 53 (1988).

Liu, J. and Gollub, J.P. "Solitary wave dynamics of film flows," *Phys. Fluid* **6**, 1702 (1994).

Liu, J., Paul, J.D. and Gollub, J.P. "Measurements of the primary instabilities of film flows," *J. Fluid Mech.* **250**, 69 (1993).

Liu, J., Schneider, J.B. and Gollub, J.P. "Three dimensional instabilities of film flows," *Phys. Fluids* **7**, 55 (1995).

Miyara, A. "Numerical simulation of wavy liquid film flowing down on a vertical wall and an inclined wall," *Int. J. Thermal Sci.*, **39**, 1015 (2000).

Nagasaki, T., Akiyama, H. and Nakagawa, H. "Numerical analysis of flow and mass transfer in a falling liquid film with interfacial waves," *Thermal Sci. & Eng.* **10**, 17 (2002).

Nagasaki, T., and Hijikata, K. "A Numerical Study of Interfacial Waves on a Falling Liquid Film," *ANS Proc. National Heat Transfer Conf.,* **4**, 23 (1989).

Nakoryakov, V.E., Pokusaev, B.G. and Alekseenko, S.V. "Effect of waves on the desorption of CO_2 from flowing liquid films," *Theor. Found. Chem. Eng.* **17**, 199 (1983).

Nishioka, M., Asai, M. and Iida, S. "Wall phenomena in the final stage of transition to turbulence," *Transition and Turbulence*, R.E. Meyer, ed., Academic Press, New York, p. 113 (1981).

Nosoko, T., Yoshimura, P.N., Nagata, T. and Oyakawa, K. "Characteristics of two-dimensional waves on a falling liquid films," *Chem. Eng. Sci.* **51**, 725 (1996).

Ooshida T. "Surface equation of falling film flows with moderate Reynolds number and large but finite Weber number," *Phys. Fluids,* **11**, 3247 (1999).

Pierson, F.W. and Whitaker, S. "Some theoretical and experimental observations of the wave structure of falling liquid films," *Ind. Eng. Chem.*, Fundam. **16**, 401 (1977).

Pumir, A., Manneville, P. and Pomeau, Y. "On solitary waves running down an inclined plane," *J. Fluid Mech.* **135**, 27 (1983).

Ramaswamy, B., Chippada, S. and Joo, S.W. "A full-scale numerical study of interfacial instabilities in thin-film flows," *J. Fluid Mech.* **325**, 163 (1996).

Roberts, R.M. and Chang, H.-C. "Wave enhanced interfacial transfer," *Chem. Eng. Sci.* **55**, 1127 (2000).

Rumscheidt, F.D. and Mason, S.G. "Break-up of stationary liquid threads," *J. Colloid Sci.* **17**, 260 (1962).

Salamon, T.R., Armstrong, R.C. and Brown, R.A. "Traveling waves on vertical films: Numerical analysis using the finite element method," *Phys. Fluids* **6**, 2202 (1994).

Seban, B.R. and Faghri, A. "Wave effects on the transport to falling laminar liquid films, *J. Heat Transfer* **100**, 143 (1978).

Tamir, A. and Taitel, Y. "Diffusion to flow down an incline with surface resistance," *Chem. Eng. Sci.* **26**, 799 (1971).

Trifonov, Yu. Ya. "Bifurcations of two-dimensional into three-dimensional wave regimes for a vertically flowing liquid film," *Fluid Dynamics* **25**, 741 (1991).

Truesdale, G.A., Downing, A.L. and Lowdan, G.F. "The solubility of oxygen in pure water and sea-water," *J. Appl. Chem.* **5**, 53 (1955).

Tsvelodub, O.Yu. and Trifonov, Yu. Ya. "Nonlinear waves on the surface of a falling film. Part 2. Bifurcations of the first-family waves and other types of nonlinear waves," *J. Fluid Mech.* **244**, 149 (1992).

Vazquez-Una, G., Chenlo-Romero, F., Sanchez-Barral, M. and Perez-Munuzuri, V. "Mass transfer enhancement due to surface wave formation at a horizontal gas-liquid interface," *Chem. Eng. Sci.* **55**, 5851 (2000).

Yih, C.S. "Stability of liquid flow down an inclined plane," *Phys. Fluids* **6**, 321 (1963).

Yoshimura P.N., Nosoko T. and Nagata T. "Enhancement of mass transfer into a falling laminar liquid film by two-dimensional surface waves - Some experimental observations and modeling," *Chem. Eng. Sci.* **51**, 1231 (1996).